Hydrodynamics forces on a circular particle near a sinusoidal corrugated wall

Zarghami, Ahad; Ashorynejad, Hamid Reza; Padding, Johan T.

DOI
10.1016/j.powtec.2018.10.052

Publication date
2019

Document Version
Final published version

Published in
Powder Technology

Powder Technology 342 (2019) 789–800

Contents lists available at ScienceDirect

Powder Technology

journal homepage: www.elsevier.com/locate/powtec

Hydrodynamics forces on a circular particle near a sinusoidal corrugated wall

Ahad Zarghami [a,*], Hamid Reza Ashorynejad [b], Johan T. Padding [a]

[a] Department of Process & Energy, Delft University of Technology, Delft, the Netherlands
[b] Department of Industrial, Mechanical and Aerospace Engineering, Buein Zahra Technical University, Buein Zahra, Qazvin, Iran

ARTICLE INFO

Article history:
Received 21 June 2018
Received in revised form 2 October 2018
Accepted 25 October 2018
Available online 27 October 2018

Keywords:
Corrugated wall
Drag
Lift
Torque
Wall effect

ABSTRACT

We study the hydrodynamic forces acting on a fixed particle close to a corrugated wall experiencing tangential fluid flow, using the lattice Boltzmann method. To carry out a fundamental analysis, a single two-dimensional circular particle near a sinusoidal wall is selected as a case study. The influence of the particle distance from the wall, the particle Reynolds number, corrugation amplitude, and downstream particle position (relative to a corrugation-peak) on the drag, lift and torque acting on the particle are investigated. Our simulations reveal that the hydrodynamic forces change significantly by changing the particle distance from the wall. Even the direction of forces and torque may change, depending on the distance from the wall, downstream particle position and Re_p number. We find an increase in magnitude of forces and torque by increasing the corrugation amplitude of the wall.

1. Introduction

Particle-fluid flows are commonly encountered in a wide range of processing equipment. An important example is fluidized bed systems [1–3] which are used for separations, rapid mass and heat transfer operations, gasification of biomass, and catalytic reactions. Fluidization occurs when solid particles are suspended by a sufficiently fast upward-flowing stream of fluid, which can be either gaseous or liquid. As a result, the particles rapidly swirl around the bed, creating excellent mixing among them and providing a large surface area for the fluid to contact [4,5]. More generally, for all particle-fluid systems, the efficiency of contacting between fluid phase and particles is dictated to a large extent by the particle dynamics which in turn has a great impact on the heat and mass transfer [1,6–8].

The fundamental physical mechanism involved in particle-fluid flows are generally complex. The drag and lift, and torque acting on a particle is not only sensitive of the flow velocity and particle size, but also of the particle shape and orientation with respect to flow [9–11]. The hydrodynamic forces are also altered by the presence of a nearby wall [12–17]. This sensitivity of a nearby wall could be used as a benefit in engineering solutions. For example, corrugated walls can be implemented as a modified geometrical configuration for the walls of processing equipment, where the corrugations create a steady vortex or swirl in the grooves. The changes in flow mixing, boundary layer disruption, and thinning will affect the hydrodynamic forces acting on particles may result in more effective designs.

To the best of our knowledge, the effect of a nearby corrugated wall on hydrodynamic forces and torque acting on a particle has not been studied before. Hence, to keep the problem as simple as possible, in this paper we investigate the effect of a sinusoidal corrugated wall on the flow and hydrodynamic forces acting on a circular particle by means of numerical modeling. The effects of some important parameters, i.e. distance from the wall, Reynolds number, corrugation amplitude and downstream particle location are investigated.

The paper is structured as follows. In Section 2, a description of the problem and the numerical method used are presented. Results are presented and discussed in Section 3, follow by our conclusions in Section 4.

2. Problem statement & numerical method

2.1. Problem description

Fig. 1 shows a schematic of the flow configuration, together with our coordinate system and the geometrical parameters adopted in this work. At the inlet, a uniform velocity, $(U_{in}, 0)$ is assumed and no-slip and free-slip boundary conditions are applied to the bottom wavy wall and top boundary of the channel, respectively. A circular particle is placed in the domain with a diameter equal to $D = 40$ lattice nodes. Effectively this represents a very long cylindrical particle, oriented perpendicular to the flow but parallel to the wall. The height and the length of the computational domain is set to $H = 15D$ and $L = 40D$. The local

* Corresponding author at: Department of Process and Energy, TU Delft, Leeghwaterstraat 39, 2628 CD, Delft, the Netherlands.
E-mail address: a.zarghami-1@tudelft.n (A. Zarghami).

https://doi.org/10.1016/j.powtec.2018.10.052
0032-5910/

Nomenclature

L	Channel length
H	Channel height
D	Particle diameter
r	Local heigth of the wavy wall
A	Amplitude of the wave
n	Number of waves
c	Location of particle center
h	Distance between c and peak of the wave
X_c	Downstream location of the particle center from inlet
Re	Reynolds number in clear channel
Re_p	Particle Reynolds number
$\vec{F}$	General force term
f_i	Distribution function
$\vec{e}_i$	Discerete velocity
f_i^{eq}	Equilibrium distribution function
τ	Relaxation time
w	Weighting factor
$\vec{u}$	Velocity
P	Pressure
ρ	Density
ν	Kinematic viscosity
$\Delta\vec{x}$	Space interval
Δt	Time interval

height of the wavy wall is expressed as $r = (A/2)\sin(2\pi nx/L)$ where A and n are the amplitude and total number of waves, respectively, so the corrugation wavelength is $\lambda = L/n$. The distance between the center of the particle, c, and the peak of the wavy wall is indicated by h. Hence, if a particle is located inside a groove of the wavy wall this will be indicated by a negative value of h. The downstream (horizontal) location of the particle center from the inlet is shown by X_c. For an empty channel, we confirmed that for our conditions the flow was sufficiently periodic (i.e. inlet effects had sufficiently decayed) after 2 wavelengths. Therefore, in our work we set X_c to at least 2λ.

The particle Reynolds number is defined as $Re_p = U_{in}D/\nu$ where ν is the fluid kinematic viscosity. In this paper, the relaxation time is fixed to $\tau = 0.56$ for all simulations. Considering the fixed size of the particle, various Re_p numbers are obtained by varying the fluid velocity U_{in}. We can define two aspect ratios characterizing the corrugation, $AR_1 = A/D$ and $AR_2 = \lambda/D$, which are the ratio of amplitude and wavelength to particle diameter, respectively. In this work, $AR_2 = 8$ for all presented simulations. Moreover, most results will be presented along two main downstream sections, (i.e. a-a & b-b), which are located at the third peak and third trough of the wavy wall in the computational domain (see Fig. 1).

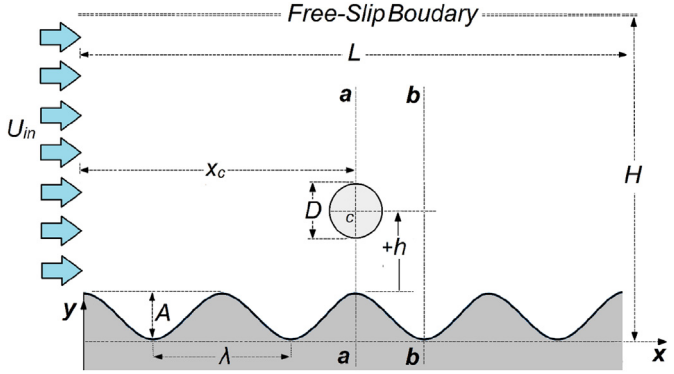

Fig. 1. Schematic of flow around a circular particle close to a sinusoidal corrugated wall.

2.2. Numerical method

The lattice Boltzmann method (LBM) is used to simulate the fluid flow. The LBM is a mesoscopic scheme based on kinetic theory. It has been applied successfully to simulate various complex fluid flow problems [18–28]. LBM has a number of advantages over conventional CFD methods, including: the simple form of the governing equations, space–time locality, straightforward parallelism, easy grid generation, and capability of incorporating complex microscopic interactions. The general lattice Boltzmann equation (LBE) with the BGK collision operator is expressed as [29]:

$$f_i\left(\vec{x}+\vec{e}_i\Delta t, t+\Delta t\right) - f_i\left(\vec{x},t\right) = -\frac{\Delta t}{\tau}\left(f_i\left(\vec{x},t\right) - f_i^{eq}(\vec{x},t)\right) \quad (1)$$

where $\vec{x}$ is a spatial coordinate, t is time, $f_i(\vec{x},t)$ is the density distribution function associated with the discrete velocity in direction i, and τ is the relaxation time of the fluid. The discrete velocities $\vec{e}_i$ in the i-direction, for the square D2Q9 lattice, are given by $\vec{e}_0 = 0$ and $\vec{e}_i = \Lambda_i(\cos\theta_i, \sin\theta_i)$ with $\Lambda_i = 1$, $\theta_i = (i-1)\pi/2$ for $i = 1-4$ and $\Lambda_i = \sqrt{2}$, $\theta_i = (i-5)\pi/2 + \pi/4$ for $i = 5-8$. The numbers $i = 1-4$ and $i = 5-8$ represent the rectangular and diagonal directions of the lattice, respectively. The equilibrium distribution function, f_i^{eq}, is defined as [29]:

$$f_i^{eq} = w_i\rho\left[1 + 3\left(\vec{e}_i.\,\vec{u}\right) + 4.5\left(\vec{e}_i.\,\vec{u}\right)^2 - 1.5\left(\vec{u}\,.\,\vec{u}\right)\right] \quad (2)$$

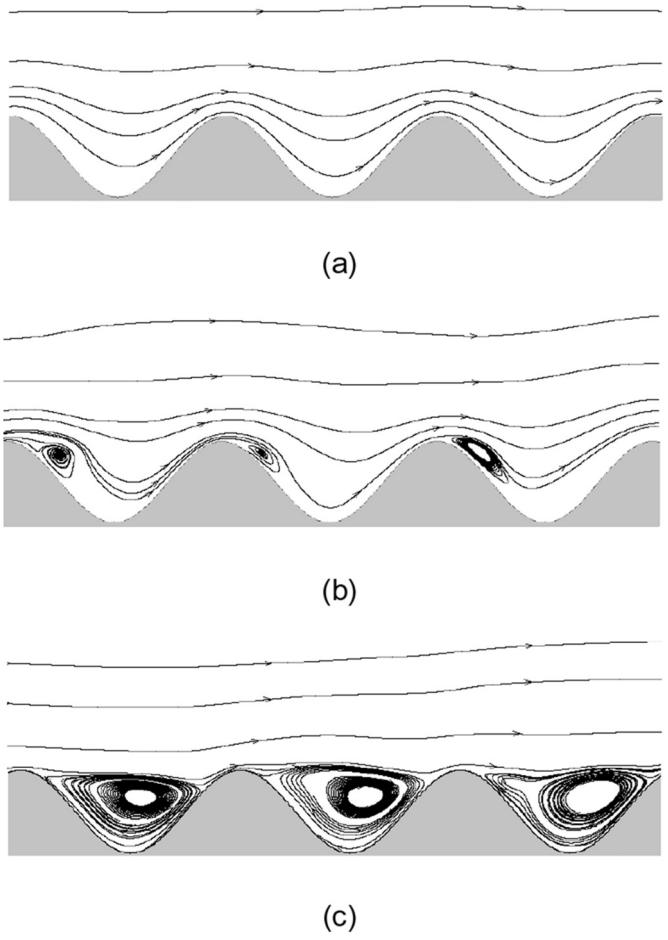

Fig. 2. Flow streamlines for a channel with a corrugated-wall at a) $Re = 10$, b) $Re = 100$ and c) $Re = 400$. Note the image is clipped to the central part of the domain.

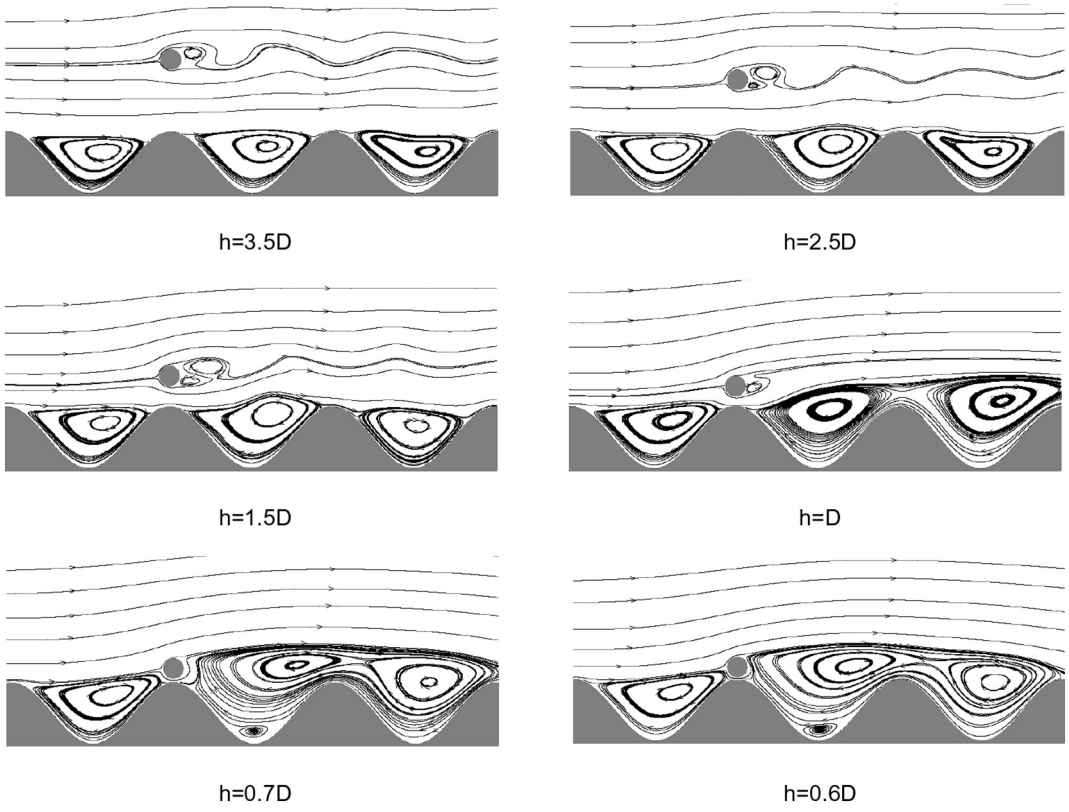

Fig. 3. Flow streamlines for a cylindrical particle in a corrugated-wall channel with $AR_1 = 3$, $AR_2 = 8$, $Re_p = 50$ for different distances, h, along the cross-section a-a. Note the image is clipped to the central part of the domain.

where $\vec{u}$ is the velocity, and w_i are the weight factors, equal to 4/9 for $i = 0$, 1/9 for $i = 1 - 4$ and 1/36 for $i = 5 - 8$. The density, viscosity, velocity and pressure are calculated as $\rho = \sum f_i$, $\nu = (\tau - 0.5)/3$, $\vec{u} = (\sum_i \vec{e}_i f_i)/\rho$ and $p = \rho/3$, respectively. The LBE is usually solved through standard collision and streaming steps where for convenience dimensionless lattice units are utilized, i.e. $\Delta \vec{x} = \Delta t = 1$. The equivalent Navier–Stokes equations, Eqs. (3) and (4) below, can be recovered from the discrete lattice Boltzmann equation under the assumption that density variations are small [29].

$$\frac{\partial \rho}{\partial t} + \nabla\left(\rho \vec{u}\right) = 0, \tag{3}$$

$$\frac{\partial}{\partial t}\left(\rho \vec{u}\right) + \nabla \cdot \left(\rho \vec{u}\vec{u}\right) = -\nabla p + \nu \nabla \cdot \left[\rho\left(\nabla \vec{u} + \left(\nabla \vec{u}\right)^T\right)\right]. \tag{4}$$

We model the surface of the particle and the corrugated wall as a no-slip boundary, using the enhanced bounce-back procedure for curved boundaries proposed by Bouzidi et al. [30]. Also, the so-called momentum exchange approach is applied for computing the fluid forces acting on the particle, as follows [31]:

$$\vec{F} = \left(\vec{F}_D, \vec{F}_L\right) = \sum_{all\ x_b} \sum_{i=1}^{8} \vec{e}_i \left[\tilde{f}_i\left(\vec{x}_b, t\right) + \tilde{f}_{\bar{i}}\left(\vec{x}_f, t\right)\right] \tag{5}$$

where $\bar{i} = -i$ and the summation is done over all boundary nodes $\vec{x}_b$, which are connected to a fluid node $\vec{x}_f$ in the i direction according to $\vec{x}_b = \vec{x}_f + \vec{e}_i \Delta t$. The total torque is calculated as:

$$T = \sum_{all\ x_b} \sum_{i=1}^{8} \left(\vec{x}_b - \vec{x}_{CM}\right) \times \vec{e}_i \left[\tilde{f}_i\left(\vec{x}_b, t\right) + \tilde{f}_{\bar{i}}\left(\vec{x}_f, t\right)\right] \tag{6}$$

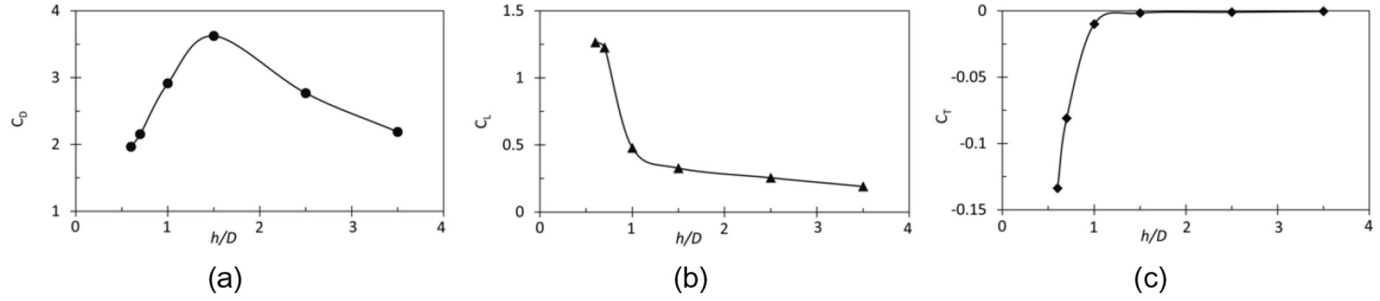

Fig. 4. Averaged a) drag force, b) lift force and c) torque coefficients as a function of particle distance from the corrugated wall along the cross-section a-a for $AR_1 = 3$, $AR_2 = 8$ and $Re_p = 50$.

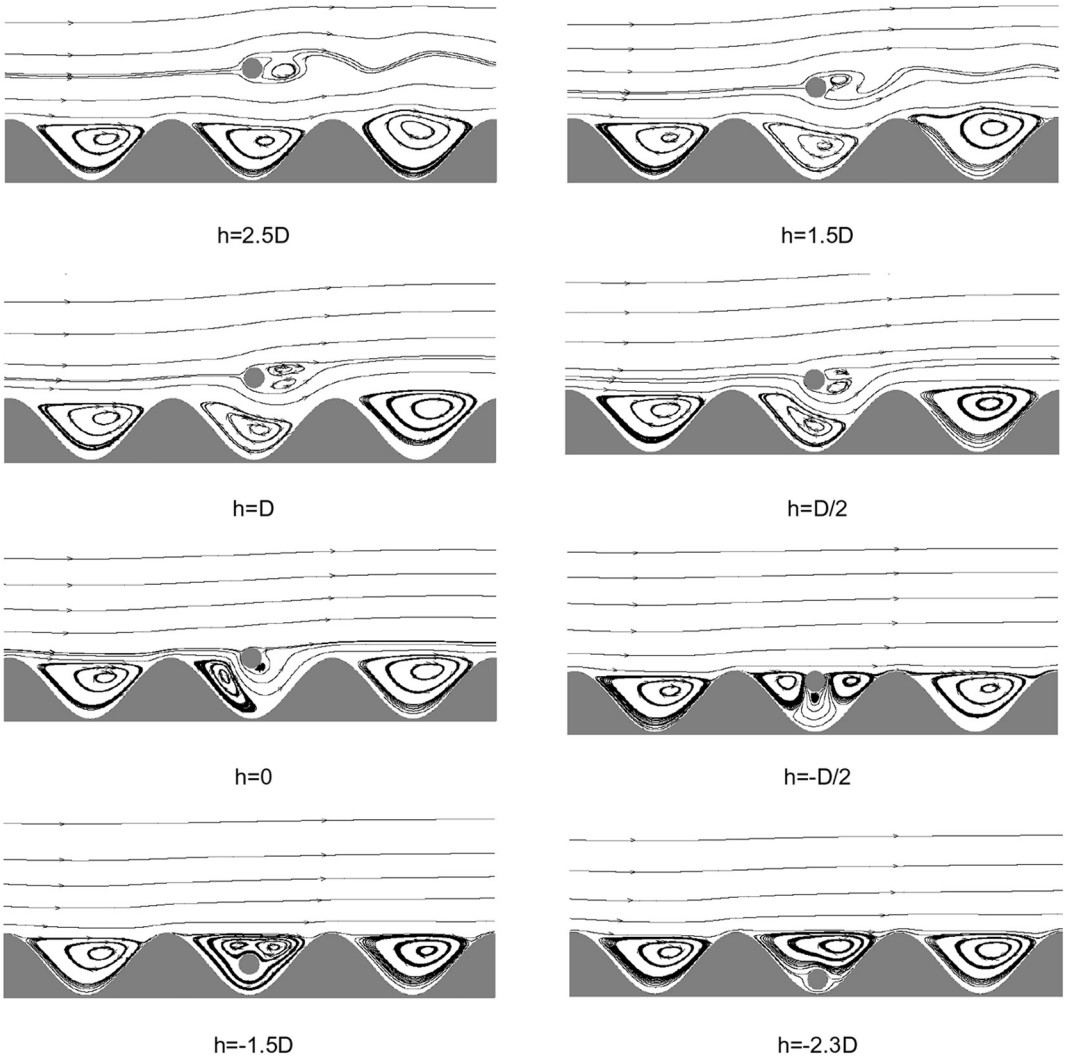

Fig. 5. Flow streamlines for a cylindrical particle in a corrugated-wall channel with $AR_1 = 3$, $AR_2 = 8$ at $Re_p = 50$ for different distances, h, along the cross-section b-b. Note the image is clipped to the central part of the domain.

where $\vec{x}_{CM}$is the center of mass of the solid object. The drag, lift and torque coefficients, respectively, are defined as:

$$C_D = \vec{F}_D / \left(0.5\rho U_{in}^2 D\right) \tag{7}$$

$$C_L = \vec{F}_L / \left(0.5\rho U_{in}^2 D\right) \tag{8}$$

$$C_T = T / \left(0.5\rho U_{in}^2 D^2\right) \tag{9}$$

The well-known Zou and He boundary condition [32] is used for the inlet boundary. For the outflow, the convective boundary condition is applied [33]. Comprehensive details of the presented numerical method, boundary conditions, and validation of the method have been presented in our previous works [17,34,35].

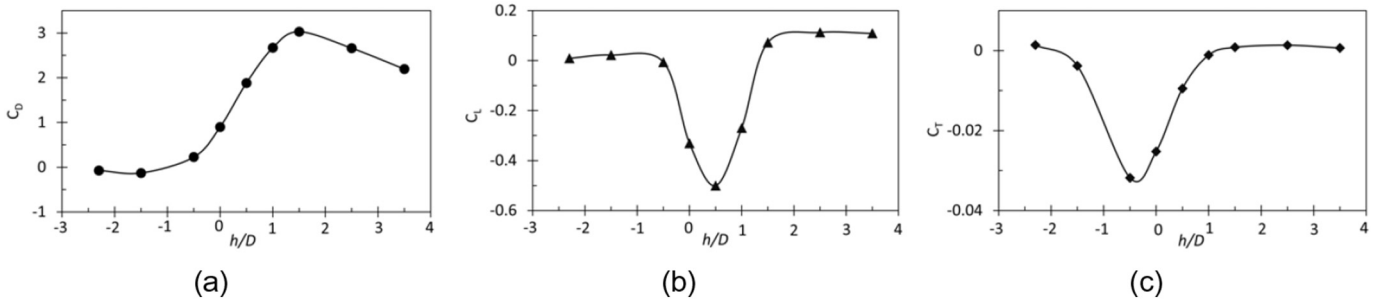

Fig. 6. Averaged a)drag force, b)lift force and c)torque coefficients as a function of particle distance from the corrugated wall along the cross-section b-b for $AR_1 = 3$, $AR_2 = 8$ and $Re_p = 50$.

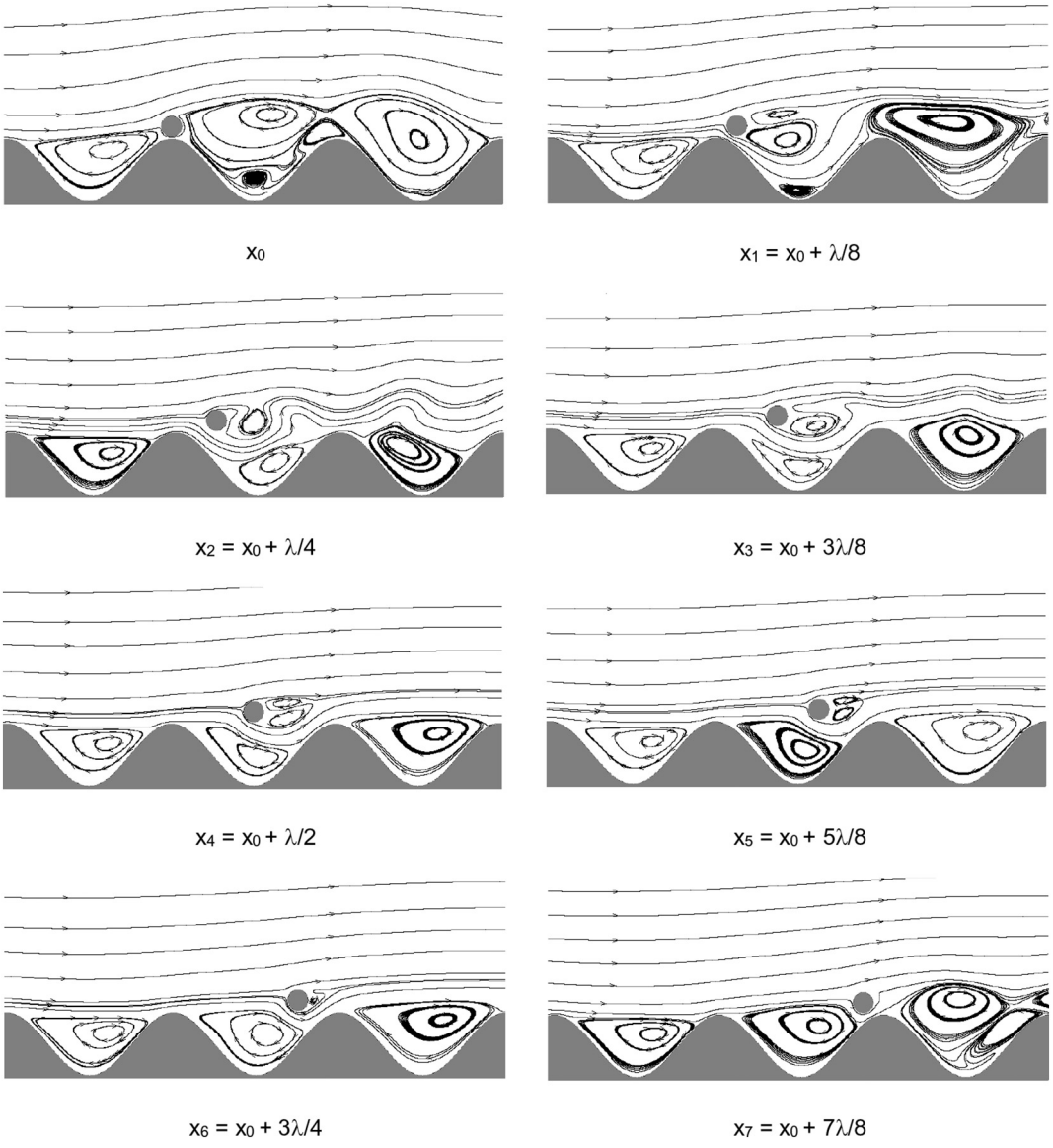

Fig. 7. Flow streamlines around the particle for different downstream particle positions for $AR_1 = 3$, $AR_2 = 8$, h = D/10 and $Re_p = 75$. Note the image is clipped to the central part of the domain.

3. Simulation results

In this section, after briefly discussing the emergence of a recirculation region in the grooves of a corrugated wall in a channel without any particle, the influence of various effective parameters, i.e. distance from the wall (h), Re_p, aspect ratios AR_1 and AR_2, and particle location (X_c) on drag, lift and torque acting on a circular particle in or near such a fully developed recirculation region are presented and discussed.

3.1. Empty corrugated channel

Fig. 2 shows the flow streamlines (clipped to a central part of the computational domain) at three different *Re* numbers (here, in the absence of a particle, we define *Re* on the basis of the channel height H: $Re = U_{in}H/\nu$). It is observed that the flow structure is fairly complex and that by increasing the *Re* number, recirculation regions form in the grooves of the wall. At low Re numbers (see Fig. 2(a)), the inertia of the flow is small and streamlines largely follow the wall shape and no recirculation region is formed. At larger Re number, the effect of viscosity becomes weakened and flow separation may occur if the Re number becomes larger than a critical value. Above the critical *Re* number, a small circulatory vortex forms behind each peak of the corrugation (see Fig. 2(b)). By further increasing *Re*, the vortices in the grooves become larger as they separate from the corrugated wall behind the peaks and

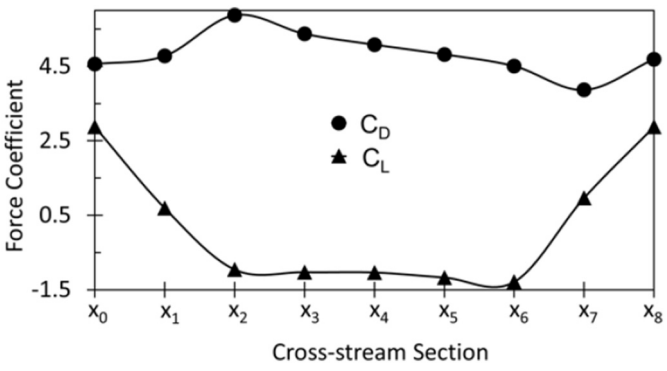

Fig. 8. Averaged drag and lift coefficients as function of streamwise displacement for in a wavy-channel with $AR_1 = 3$, $AR_2 = 8$ and $Re_p = 50$.

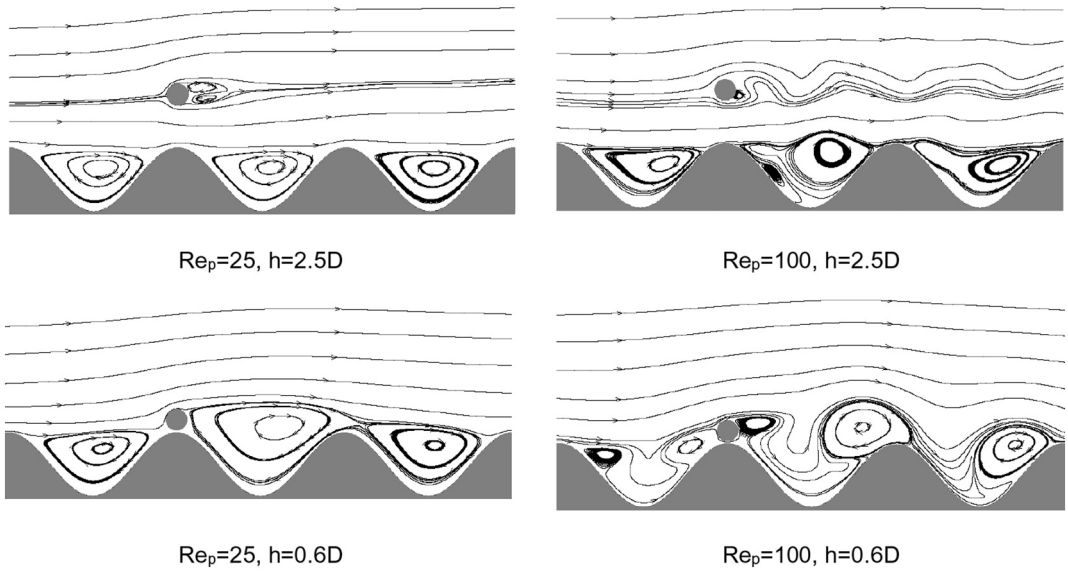

Fig. 9. Flow streamlines around the cylindrical particle at two Re_p numbers and two heights h from the wall along the cross-section a-a; $AR_1 = 3$, $AR_2 = 8$. Note the image is clipped to the central part of the domain.

reattach right before the peaks (see Fig. 2(c)). In this case, the recirculation zones tend to fill the whole groove and their vortex center shifts downstream.

The recirculation region is the major feature of a flow near a corrugated wall [36]. Compared to the flow near a flat wall, this feature results in backflow (at large *Re*), streamline curvature and non-zero wall-normal velocity near the corrugated channel. These non-zero wall-normal mean velocities and their non-negligible spatial gradients play a significant role in momentum, heat, mass transport and flow mixing, which is not possible in a channel with flat walls. In the remainder of this paper we will focus on the situation of a fully developed recirculation region (corresponding to Fig. 2c).

3.2. Effect of gap size

To show the effect of particle distance from the wall on hydrodynamic forces and torque, we focus on the flow around a circular particle near a corrugated wall with $AR_1 = 3$, $AR_2 = 8$ and $Re_p = 50$. Note that because H = 15D, the channel Reynolds number is higher: $Re = H/D\ Re_p = 750$, which is sufficiently high to warrant a fully developed recirculation region in each groove. Fig. 3 shows the streamlines in the center of the computational domain around the particle at various distances from the wall along the cross-section a-a, i.e. at a downstream position equal to a peak position of the corrugated wall. It can be seen that when the particle is far from the wall (i.e. h ≥ 1.5D), the flow around the particle closely resembles that of an isolated circular cylinder, with the well-known von-Karman vortex shedding occurring behind the particle. Also, it is clear that no significant interaction is observed between the von-Karman vortex shedding and vortices in the grooves. When the particle gets closer to the wall, i.e. at h < 1.5D, the von-Karman vortex street behind the particle is strongly affected by the presence of the wall. For very small distances from the wall (h = 0.7D, h = 0.6D), the particle more resembles an obstacle to the fluid flow. As a result, the von-Karman vortex shedding is suppressed and a large and complex recirculation region is formed behind the particle. For these cases, a secondary small recirculation region appears in the lowest part of the first downstream groove.

The dependencies of the average drag force, lift force and torque coefficients on the distance from the wall are presented in Fig. 4(a), 4(b) and 4(c), respectively. Generally, the drag force is independent of the particle location when the particle is far from the wall (i.e. h > 10D). Our results show that the drag increases by decreasing the distance from the wall due to the added viscous effect arising from the presence of the wall. However, by further decreasing the distance from the wall to h < 1.5 D, the drag force decreases. In these cases, the effect of wall is to slow down the flow in the gap between the particle and the wall, which results in a reduced viscous friction on the wall facing side of the particle.

The lift force tends to zero when the particle distance from the wall is large, as for distances of the order of 10D, the wall-proximity effect can be ignored [37]. Fig. 4(b) shows that by decreasing the distance h, the lift force increases significantly. The presence of a wall breaks the

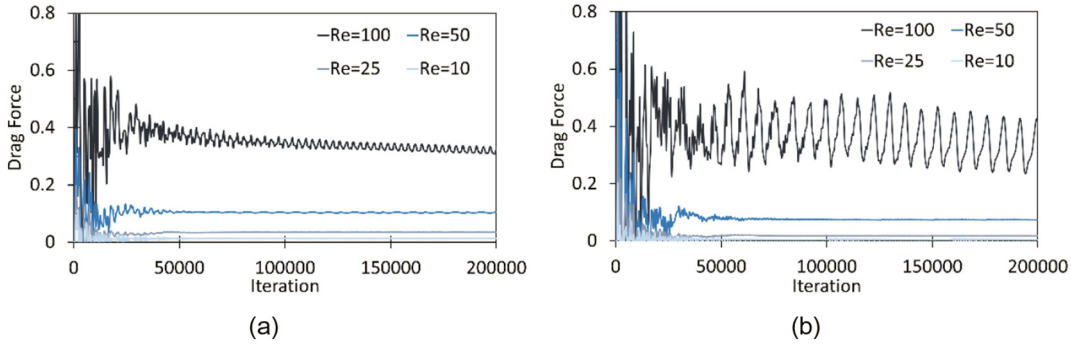

Fig. 10. Time-dependent drag force acting on a cylindrical particle with $AR_1 = 3$, $AR_2 = 8$ at different Re_p numbers for a) h = 2.5D, b) h = 0.6D along the cross-section a-a.

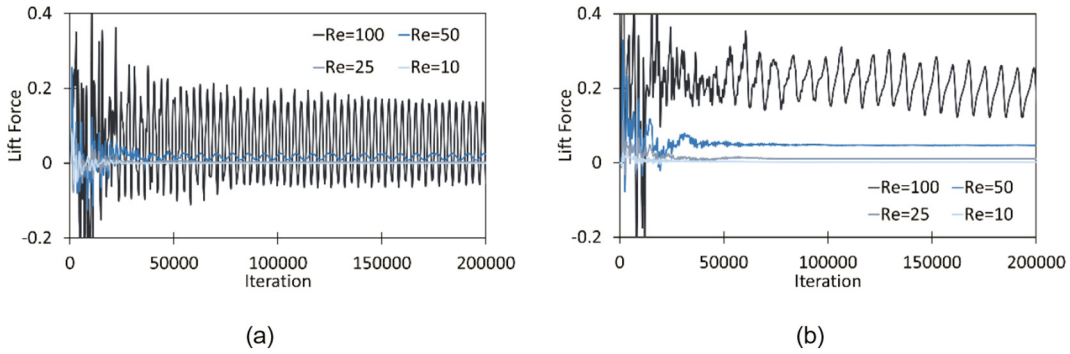

Fig. 11. Time-dependent lift force acting on a cylindrical particle with $AR_1 = 3$, $AR_2 = 8$ at different Re_p numbers for a) h = 2.5D, b) h = 0.6D along the cross-section a-a.

symmetry of the generated wakes behind the particle, which generally results in an effective lift force directed away from the wall. By decreasing the distance between the particle and the wall, the wall-induced lift, due to the interaction between the vorticity generated at the particle surface and the surface of the wall, becomes pronounced.

Similar to the lift force, the torque on the particle approaches zero when the distance from the wall is large, see Fig. 4(c). However, for small distances from the wall (i.e. h < D), the particle experiences a negative (clockwise) torque. Fig. 3 shows that the size of the vortex area behind the particle and the effect of the wall on its symmetry breaking becomes pronounced, resulting in an enhancement of the torque. We note that the lower shear layer on the particle interacts with the wall shear layer when the distance becomes small and a larger vortex is formed behind the particle. The negative wall shear layer cancels part of the vorticity in the positive lower shear layer of the particle, thus the lower shear layer is weakened. Consequently, the separated positive lower shear layer is not strong enough, whereas the negative upper shear layer is strong enough to roll up to form a vortex. This phenomenon results in a negative torque acting on the particle.

Fig. 5 shows the variations of flow streamlines when the particle approaches to the corrugated wall along the cross-section b-b normal to the deepest groove of the wall with $AR_1 = 3$, $AR_2 = 8$ and $Re_p = 50$. When the particle is far from the groove, regular vortex shedding occurs behind the particle. In this case, the flow in the groove region is similar to a lid-driven sinusoidal cavity flow as a large vortex fills the groove. When the particle gets closer to the groove (i.e. h ≤ D), the von-Karman vortex behind the particle and the recirculation region in the groove interact. For h = 0, the particle enters the recirculation region in the groove and shifts its core toward the upper left corner of the cavity and also the vortex shedding behind the particle is suppressed. By decreasing the distance to h = −D/2, the recirculation region in the groove is divided into two main but smaller regions positioned left and right of the particle. A small eddy zone is also formed at the bottom surface of the particle. For h = −1.5D, the particle is located in the center of the cavity, and is surrounded by the recirculation region. By further decreasing the distance (i.e. h = −2.3D), the particle is positioned very close to the boundary of the wall and the recirculation region mainly forms above the particle.

Fig. 6(a) shows the dependence of the average drag force coefficient on the distance h when the particle is located along the cross-section b-b, corresponding to Fig. 5. Compared to the cross-section a-a, when the particle approaches the groove, the fluid now has more freedom to flow underneath the particle. This leads to a slightly smaller drag force (at the same h as for cross-section a-a), but similarly, the drag force increases as the particle gets closer to the wall down to h = 1.5D. As the particle-wall distance decreases below h = 1.5D, the shedded von-Karman vortices of the particle interact with the recirculation region in the groove. The size of the vortex behind the particle decreases significantly by decreasing the distance (i.e. h = D and D/2, see Fig. 5) and finally the vortex shedding is suppressed for h = 0. By shrinking and finally eliminating the vortex shedding, the contribution of the pressure drag is reduced, resulting in a decrease in net drag force acting on the particle. As shown in Fig. 5, by further decreasing the distance to h = −D/2, two co-rotating wakes form on the left and right side of the particle. Due to the opposite sign of the flow velocity at the left and right sides of the particle, the friction drag acting on the two sides cancel each other, resulting in a further decrease of the net drag force. For smaller values of h, i.e. h = −1.5D, the particle is entirely located within the recirculation region of the groove, leading to a negative drag force. Because the magnitude of the velocity within the groove is about one order of magnitude smaller than the free-stream velocity, the magnitude of this negative drag is small. At very small distance, i.e. h = −2.3D, the particle is very close to the stationary wall of the groove and as a result the negative drag force increases toward zero again. This increase in drag force can be justified in terms of the added viscous effect arising from the presence of the wall.

Fig. 6(b)shows that the average lift force is close to zero when the particle is far from the groove (h ≥ 2.5D). Decreasing the distance below h = 1.5D, a negative lift force is experienced by the particle. It should be mentioned that the wall-induced lift force is due to two

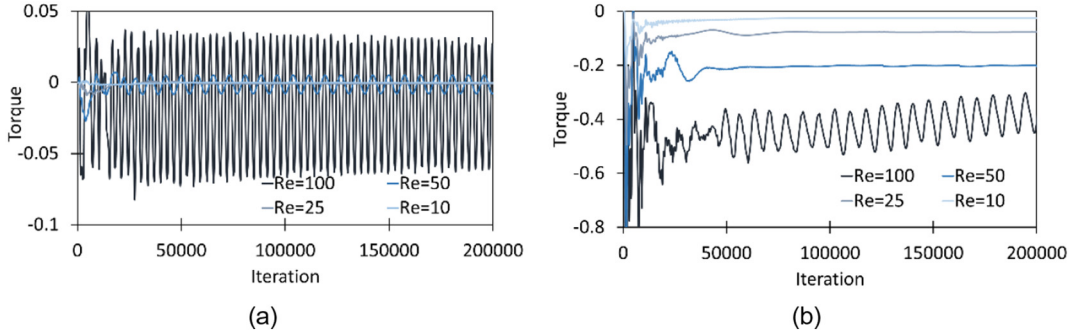

Fig. 12. Time-dependent torque acting on a cylindrical particle with $AR_1 = 3$, $AR_2 = 8$ at different Re_p numbers for a) h = 2.5D, b) h = 0.6D along the cross-section a-a.

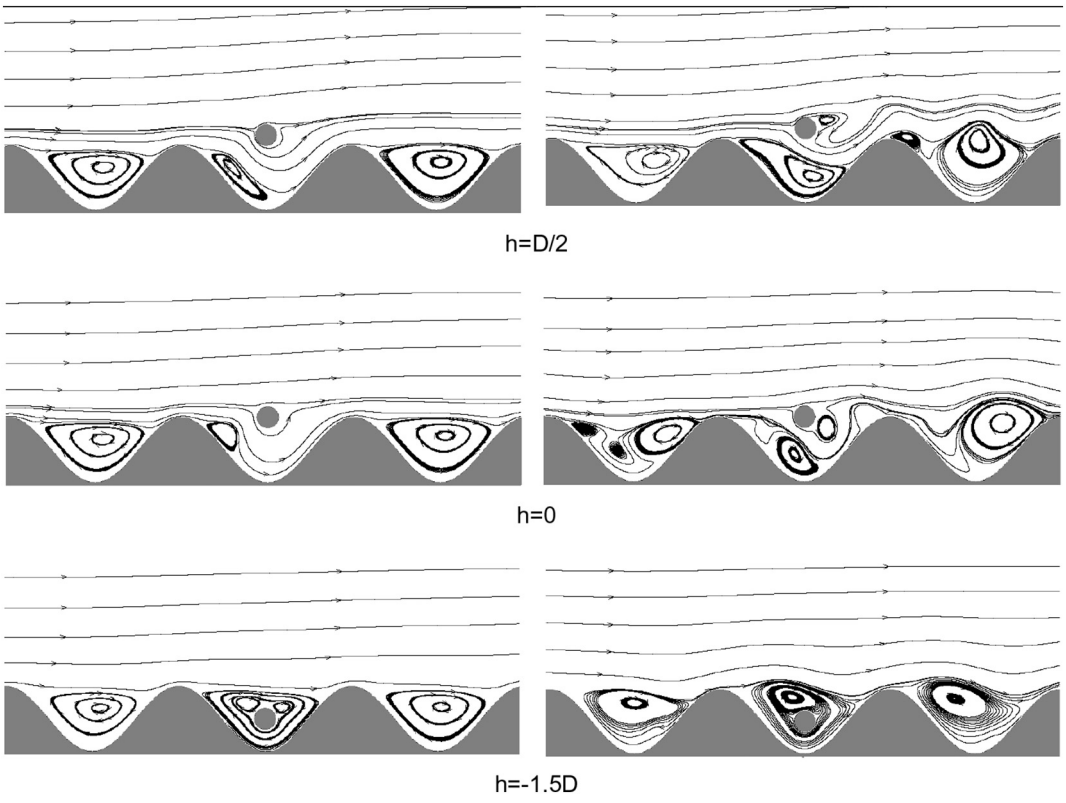

Fig. 13. Flow streamlines around the cylindrical particle at two different *Re* numbers and different distances from the wavy-wall with $AR_1 = 3$, $AR_2 = 8$, along the cross-steam section b-b. Note the image is clipped to the central part of the domain.

mechanisms. The vorticity generated at the particle surface advects downstream, interacts with the wall, and results in a lift force directed away from the wall (i.e. with positive sign). On the other hand, the fluid is accelerated in the gap between the particle and the wall in the limit of an inviscid flow. This effect results in a local low pressure region in the gap, corresponding to a negative net lift force directed toward the wall. Usually for flow in a channel with straight walls, the wall-induced lift due to the symmetry breaking of vortices is the dominant phenomenon. However, in our case study, as shown in Fig. 5, the vortex region generated behind the particle becomes smaller as the particle gets closer to the groove. Hence, by decreasing the distance from $h = 1.5D$ to $h = 0.5D$, the positive wall-induced lift force becomes smaller compared to the wall-directed lift force, resulting in a negative lift force on the particle. Furthermore, the recirculation flow in the groove applies a negative lift on the particle by pulling the particle into its core. By further decreasing the distance, i.e. $h \leq 0$, the particle enters into the groove and its recirculation region with small velocity magnitude. Hence, the magnitude of the lift force decreases and approaches zero as the particle gets very close to the bottom of the groove.

As shown in Fig. 6(c), the average torque acting on the particle starts from a value close to zero when the particle is far from the groove (i.e. $h > D$), and then becomes negative as the distance decreases. The reason for the negative torque is that the positive shear layer on the lower surface of the particle interacts with the top shear layer of the recirculation region in the groove with the negative sign and cancel each other out to some extent. Hence, the negative shear layer on the upper side of the particle is the dominant mechanism, which results in a negative torque (leading to clockwise rotation) of the particle. Furthermore, when the particle is located close to the groove, the vorticity of the recirculation region will effectively apply a negative torque on the particle. These mechanisms become stronger as the distance decreases from $h = D$ to $h = -D/2$. However, by further decreasing the distance ($h < -D/2$),

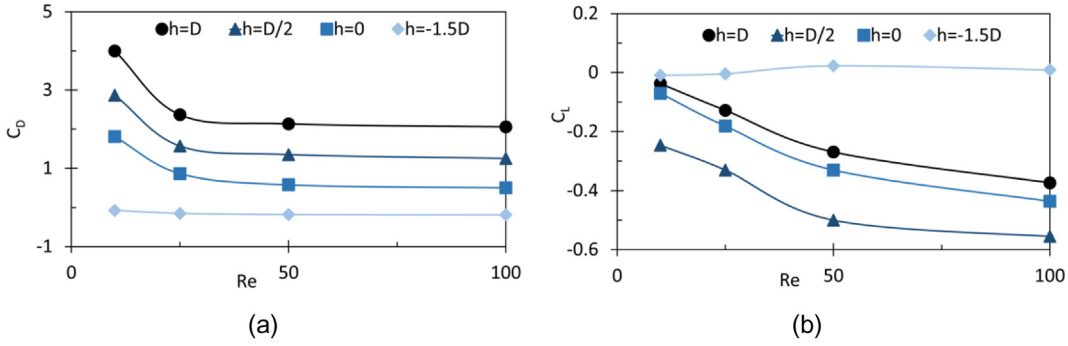

Fig. 14. Averaged a) drag force and b) lift force coefficients as function of Re_p number for flow around a cylindrical particle near a sinusoidal wall with $AR_1 = 3$, $AR_2 = 8$ and different distances from the wall along cross-section b-b.

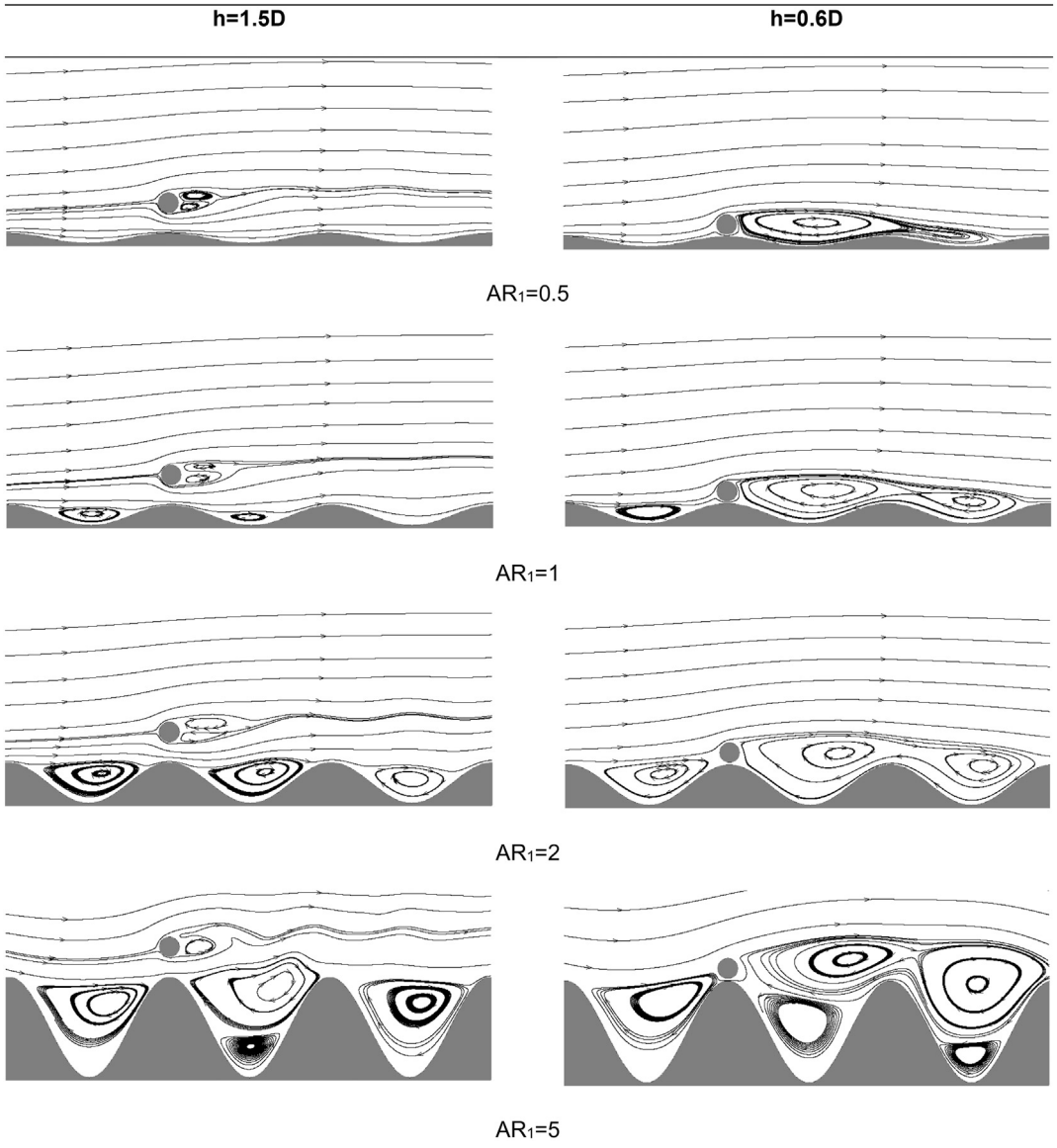

Fig. 15. Streamlines patterns for different wall corrugation amplitude AR_1 and two different distances from the wall (left panels: h = 1.5D, right panels: h = 0.6D) along cross-section a-a for $AR_2 = 8$, $Re_p = 50$. Note the image is clipped to the central part of the domain.

the magnitude of the torque decreases and tends to zero. At such close distances, the particle is located completely inside the recirculation region with a small velocity magnitude and no vortex is formed around the particle to interact with the wall. Therefore, the magnitude of the torque acting in the particle decreases dramatically.

3.3. Effect of downstream particle position

To further study the effect of the recirculation region in the groove on the hydrodynamic forces acting on a particle, we place the particle at different downstream locations, at a constant height h. For this

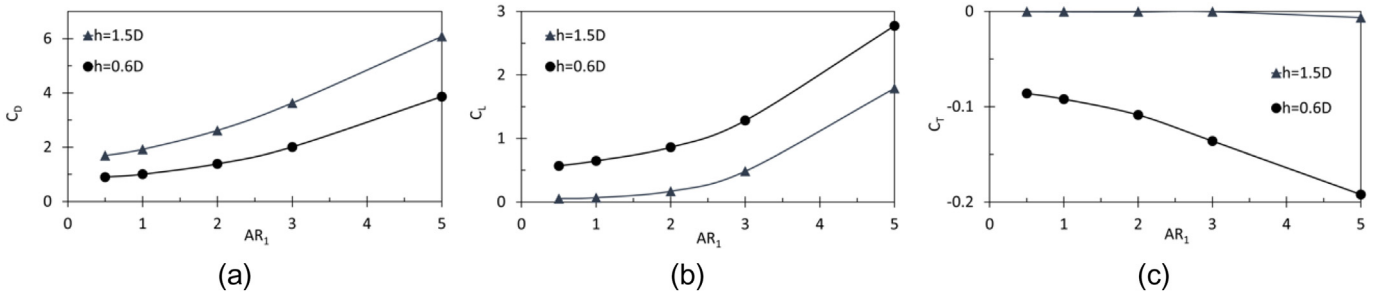

Fig. 16. Averaged a) drag, b) lift and c) torque coefficients as function of waviness amplitude (AR_1) for two different distances from the wall, along the cross-section a-a, for $AR_2 = 8$, $Re_p = 50$.

purpose, we start with the particle at the peak of a wave (downstream location x_0), with $AR_1 = 3$, $AR_2 = 8$ and $h = D/10$, and subsequently change its location with steps of $\lambda/8$ to the next downstream peak (locations x_1 to x_7). Flow streamlines for these particle locations are shown in Fig. 7. When the particle is located at x_0, it acts like an obstacle to the fluid flow and most of the fluid is directed over the top of particle. As a result, a large and complex wake region is formed behind the particle and in the next two grooves downstream. When the particle is located at x_1 or x_2 the fluid flows more easily along the bottom of the particle. Hence, some vortex-shedding occurs behind the particle, reducing the size of the recirculation region in the groove. By further moving the particle downstream, the vortex shedding is affected by the converging part of the wavy wall: already at x_3 the vortex shedding becomes weakened. At x_4, the effect of the converging section of the groove is quite strong as the vortex shedding is completely suppressed and two steady vortices of unequal size are formed behind the particle. On the other hand, the recirculation region in the groove becomes pronounced and occupies most of the area of the groove. When the particle approaches the next top of the wave, the size of the steady state wakes is further affected by the converging wall, resulting in smaller wakes. Finally, at x_7 the wakes are completely suppressed and again the particle acts like an obstacle to the fluid flow.

Fig. 8 shows the average drag and lift force coefficients of the particle as a function of downstream position. The drag force increases from x_0 to x_2 due to the increasing importance of vortex-shedding. For these cases, the pressure drag is the main contribution to the drag force, resulting in an increase in the drag force. As mentioned above, from x_3 to x_7 the vortex shedding is weakened. This decreases the contribution of the pressure drag, resulting in a monotonic decrease in total drag force. Finally, at x_8 (equivalent to x_0) the drag force increases again due to the added viscosity effect of the adjacent wall.

The particle experience a positive lift at x_0 due to the existence of the solid wall. At x_1, the particle is far enough from the wall surface and vortex-shedding is easily formed. As a result, the lift force tends to zero. At x_2 to x_6, the lift force has a negative and approximately constant value. At these particle locations, the effect of the wall on symmetry-breaking is not significant, hence the negative wall-directed lift force due to the existence of the recirculation region in the groove is dominant. When approaching the next wave peak, the effect of wall-proximity on the lift force becomes pronounced again, resulting in positive lift force at x_7 and x_8.

3.4. Effect of Re_p number

In this section, the effect of the particle Reynolds number on flow hydrodynamics is studied for a wavy-channel with $AR_1 = 3$ and $AR_2 = 8$. In Fig. 9, streamlines for two different particle Reynolds numbers ($Re_p = 25$ and 100) and two different heights h (h = 2.5D and 0.6D) along the cross-section a-a are shown. When the particle is far from the wall (here h = 2.5D, top panels in Fig. 9), the flow around the particle resembles that of around an isolated cylinder. At this distance, two steady-state wakes are formed behind the particle at $Re_p = 25$ and von Karman vortex shedding occurs at $Re_p = 100$. Note that at $Re_p = 25$, the wakes behind the particle are not exactly symmetric, which is due to the existence of the wall. Also, steady and unsteady recirculation regions are formed within the wall's grooves downstream of the particle at $Re_p = 25$ and 100, respectively.

When the particle is located closer to the wall, the interaction between the wakes behind the particle and the recirculation regions in the wall's grooves becomes stronger. For h = 0.6D (bottom panels in Fig. 9) the wakes and recirculation regions have merged. As a result, a double steady-state wake is formed behind the particle at $Re_p = 25$, covering two grooves, whereas a complex vortex shedding occurs at $Re_p = 100$, affecting fluid flow in multiple grooves upstream and downstream of the particle.

The effect of Re_p number on fluctuations in the time-dependent drag force at h = 2.5D and h = 0.6D, along the cross-section a-a, is shown in Figs. 10(a) and 10(b), respectively. The drag force is approximately steady (in time) when Re_p is small, but becomes periodic at higher Re_p due to the vortex shedding. A periodic drag force is associated with periodic formation of vortical wake structures behind the particle. From animations of the system, we observed that when the flow is periodic, the frequency of vortex shedding decreases when the particle is located closer to the wall. When the particle is close to the wall, the shear layer from the lower side of the particle interacts with the shear layer of the wavy wall with an opposite sign, and is weakened and not able to form a vortex. Hence, the vortex sheds only from the upper side of the particle which interacts strongly with the wavy wall. This phenomenon affects the frequency and amplitude of the drag force on the particle.

The lift force and torque acting on the particle are show in in Figs. 11 and 12, respectively. When the particle is located far from the wall (here h = 2.5D), the lift force oscillates regularly due to the vortex shedding phenomenon at higher Re_p numbers. Generally, by decreasing the distance of the particle to the wall, the amplitude of the periodic lift force reduces due to the existence of the wall. This affects the regularity in the time dependence of the lift force as the peaks of the fluctuating lift force become irregular at higher Re_p numbers (here: $Re_p = 100$) and the regular oscillation of the lift force disappears completely at lower Re_p numbers (here: $Re_p = 50$).

When Re_p is small, the size of wake (or vortex shedding) behind the particle is small and the effect of the wall on the wake region is not high, resulting in a small torque acting on the particle. By increasing the Re_p number, the interaction between wakes behind the particle and the wavy wall becomes stronger and consequently the effect of symmetry breaking due to the existence of the wall becomes pronounced. This results in an increase in the magnitude of the torque.

Next, we investigate the influence of Re_p when the particle is located near the deepest part of the groove, i.e. along cross-section b-b in Fig. 1. Fig. 13 shows the streamlines for flow around the cylindrical particle at $Re_p = 25$ and 100 in a wavy channel with $AR_1 = 3$ and $AR_2 = 8$ for h = D/2 (top panels), h = 0 (middle panels) and h = −1.5D (bottom panels). When Re_p is small ($Re_p = 25$), the streamlines tend to be laminar and the recirculation regions within the grooves are almost steady. As Re_p increases ($Re_p = 100$), unsteady vortex shedding occurs, and the size of recirculation regions in the grooves increases. Hence the interaction between the recirculation regions and wakes behind the particle increases, and the flow becomes more disturbed.

The effect of Re_p number on drag and lift force coefficients for a particle in the vicinity of a wavy wall with $AR_1 = 3$ and $AR_2 = 8$, at different positions along cross-section b-b, is shown in Figs. 14 (a) and 14(b), respectively. For all presented distances from the wall, a larger Re_p number leads to a lower average drag coefficient, indicating the reduced role of viscosity. When the particle is above the groove (i.e. h ≥ 0), with increasing Re_p the wake behind the particle grows quickly and interacts with the flow in the grooves more strongly. Under these conditions, the pressure drag becomes the main contribution to the drag force. When the particle is located within the groove (i.e. h = −1.5D), a recirculation region forms around the particle (see Fig. 13, bottom panels). By increasing the Re_p number, this recirculation region and corresponding pressure drag becomes more pronounced. Note that in this case, the particle experiences a weak negative drag force due to the direction of velocity in the recirculation region around the particle.

Like the drag force, the magnitude of the wall-induced lift coefficient varies significantly as Re_p increases (see Fig. 14(b)). As we discussed in Section 3.2, the recirculation region in the furrow tends to rotate the particle clockwise (i.e. negative torque) and pull it to the core of the recirculation region. Hence, a negative lift is felt by the particle. At higher Re_p numbers, the size and strength of the recirculation region grows which leads to an increase in lift force coefficient.

3.5. Effect of corrugation amplitude (AR_1)

We now investigate the effect of amplitude of the wall corrugation on the hydrodynamics of fluid flow around the particle. The streamlines of fluid flow around the particle at $Re_p = 50$ and two different distances from the wavy wall, along cross-section a-a with different corrugation amplitudes, are shown in Fig. 15. It is clear that the flow streamlines strongly depend on the amount of corrugation of the channel. For small amplitude channels, i.e. $AR_1 = 0.5$, the streamlines closely follow the channel shape. By increasing the wall amplitude to $AR_1 = 1$, flow separation occurs in the grooves. As the amplitude increases further, i.e. $AR_1 = 2$, the size of the recirculation regions increases and its core is shifted to the right due to viscous effects. When $AR_2 = 5$, a secondary recirculation region is observed at the bottom of the grooves. The size of this secondary recirculation region becomes larger by further increasing the amplitude of the wall while the primary vortex becomes flatter near the crest of the wave.

If the particle is located far from the wall (left panels in Fig. 15), the wake behind the particle does not significantly interact with the wavy wall, forming similar recirculation regions for different wall corrugation amplitudes. On the other hand, at small distances from the wall (right panels in Fig. 15), the vortices shed behind the particle interact strongly and merge with the downstream recirculation regions of the wall. As a result, a large and complex vortex is formed behind the particle, covering multiple wave lengths. It can be observed that the complex vortex behind the particle expands in size as the amplitude increases.

The dependencies of the average drag force, lift force and torque coefficients on the wall corrugation amplitude for $Re_p = 50$ are presented in Figs. 16(a), 16(b)and 16(c), respectively. It can be seen that the drag coefficient increases with increasing the amplitude (AR_1) for both presented distances from the wall. As shown in Fig. 15, by increasing the corrugation amplitude, the vortex region behind the particle interacts more strongly with the recirculation regions in the downstream grooves and becomes larger and more complex. Consequently, the pressure drag increases. A similar trend is observed for the lift coefficient. The larger the corrugation amplitude, the higher the lift coefficient. The reason is that by increasing the amplitude, the effect of symmetry breaking due to the existence of the wavy wall and its recirculation regions becomes more pronounced and the magnitude of lift force directed away from the wall increases.

It can be seen from Fig. 16(c) that the magnitude of the average torque coefficient of the particle increases as the wall corrugation amplitude increases. As mentioned earlier, due to the existence of the wall the lower shear layer on the particle is interacting with the wavy wall shear layer. This interaction is pronounced as the wake region becomes larger in size due to the increase in corrugation amplitude. The negative wall shear layer cancels part of the vorticity in the positive lower shear layer of the particle, thus the lower shear layer is weakened. As a consequence, the separated positive lower shear layer is not strong enough, whereas the negative upper shear layer is strong enough to roll up to form a vortex. This phenomenon results in a negative torque on the particle. This interaction becomes stronger as the amplitude (distance from the wall) increases (decreases) resulting in torque with larger magnitude.

4. Conclusion

In many engineering applications, particles move past corrugated walls. Surprisingly little is known about the effects of such walls on the hydrodynamic forces experienced by the particles. In this paper, we considered the simplest conceivable case of a fixed two-dimensional cylindrical particle near a sinusoidal wall. By means of the lattice Boltzmann method, we solved the flow field and measured the effect of particle distance from the wall, particle downstream position, Re_p number and wall corrugation amplitude on the drag, lift and torque experienced by the particle. Our study showed that the presence of a wavy wall significantly changes the hydrodynamic forces and torque acting on the particle, as an increase or decrease of the hydrodynamic forces and torque depend on the particle distance from the wall as well as its downstream location with respect to the peak location of the wavy wall. The direction of forces and torque change, depending on particle distance from the crest or trough of a wave. Also, it was shown that a particle close to a wall with larger corrugation amplitude experiences larger hydrodynamic forces and torque, whatever the gap size.

Acknowledgment

This work was done as a part of research funded by the European Research Council (ERC) under the consolidator grant scheme, contract no. 615096 (NonSphereFlow).

References

[1] W. Zhong, A. Yu, X. Liu, Z. Tong, H. Zhang, DEM/CFD-DEM modelling of nonspherical particulate systems: theoretical developments and applications, Powder Technol. 302 (2016) 108–152.
[2] Z.Y. Zhou, D. Pinson, R.P. Zou, A.B. Yu, Discrete particle simulation of gas fluidization of ellipsoidal particles, Chem. Eng. Sci. 66 (2011) 6128–6145.
[3] V. Verma, N.G. Deen, J.T. Padding, J.A.M. Kuipers, Two-fluid modeling of three-dimensional cylindrical gas–solid fluidized beds using the kinetic theory of granular flow, Chem. Eng. Sci. 102 (2013) 227–245.
[4] Y. Tsuji, T. Kawaguchi, T. Tanaka, Discrete particle simulation of two-dimensional fluidized bed, Powder Technol. 77 (1) (1993) 79–87.
[5] P. Basu, Combustion and Gasification in Fluidized Beds, CRC Press, USA, 2006.
[6] A. Gómez-Barea, B. Leckner, Modeling of biomass gasification in fluidized bed, Prog. Energ. Combust. 36 (4) (2010) 444–509.
[7] X. Li, M. Liu, Y. Li, Hydrodynamic behavior of liquid–solid micro-fluidized beds determined from bed expansion, Particuology 38 (2018) 103–112.
[8] R.R. Palkar, V. Shilapuram, Detailed parametric design methodology for hydrodynamics of liquid–solid circulating fluidized bed using design of experiments, Particuology 31 (2017) 59–68.
[9] M. Zastawny, G. Mallouppas, F. Zhao, B. Van Wachem, Derivation of drag and lift force and torque coefficients for non-spherical particles in flows, Int. J. Multiphase Flow 39 (2012) 227–239.
[10] R. Ouchene, M. Khalij, B. Arcen, A. Tanière, A new set of correlations of drag, lift and torque coefficients for non-spherical particles and large Reynolds numbers, Powder Technol. 303 (2016) 33–43.
[11] S.K.P. Sanjeevi, J.T. Padding, On the orientational dependence of drag experienced by spheroids, J. Fluid Mech. 820 (2017) R1.
[12] Z. Zhou, G. Jin, B. Tian, J. Ren, Hydrodynamic force and torque models for a particle moving near a wall at finite particle Reynolds numbers, Int. J. Multiphase Flow 92 (2017) 1–19.
[13] L. Zeng, F. Najjar, S. Balachandar, P. Fischer, Forces on a finite-sized particle located close to a wall in a linear shear flow, Phys. Fluids 21 (3) (2009), 033302.
[14] L. Zeng, S. Balachandar, P. Fischer, Wall-induced forces on a rigid sphere at finite Reynolds number, J. Fluid Mech. 536 (2005) 1–25.
[15] T. Tsuji, E. Narita, T. Tanaka, Effect of a wall on flow with dense particles, Adv. Powder Technol. 24 (2) (2013) 565–574.
[16] S.Y. Lee, J.Y. Hyun, Analysis of force acting on the non-spherical particle near a wall, Biomed. Eng. Lett. 5 (4) (2015) 289–295.
[17] A. Zarghami, J.T. Padding, Drag, lift and torque acting on a two-dimensional non-spherical particle near a wall, Adv. Powder Technol. 29 (6) (2018) 1507–1517.
[18] S. Mukherjee, A. Zarghami, C. Haringa, K. van As, S. Kenjereš, H.E.A. Van den Akker, Simulating liquid droplets: a quantitative assessment of lattice Boltzmann and volume of Fluid methods, Int. J. Heat Fluid Flow 70 (2018) 59–78.
[19] M. Sheikholeslami, M. Gorji-Bandpy, D.D. Ganji, Numerical investigation of MHD effects on Al2O3–water nanofluid flow and heat transfer in a semi-annulus enclosure using LBM, Energy 60 (2013) 501–510.
[20] S. Di Francesco, et al., Wall roughness effect in the lattice Boltzmann method, AIP Conf. Proc. 1558 (1) (2013) 1677–1680.
[21] A. Zarghami, H.E.A. Van den Akker, Thermohydrodynamics of an evaporating droplet studied using a multiphase lattice Boltzmann method, Phys. Rev. E 95 (4) (2017), 043310.
[22] M. Sheikholeslami, D.D. Ganji, Entropy generation of nanofluid in presence of magnetic field using lattice Boltzmann method, Physica A 417 (2015) 273–286.
[23] A.S. Dogonchi, et al., Non-spherical particles sedimentation in an incompressible Newtonian medium by Padé approximation, Powder Technol. 278 (2015) 248–256.
[24] A. Kardani, P. Omidvar, A. Zarghami, Analysis of thermal flow in a rotating porous U-turn duct using lattice Boltzmann method, Transport Porous Med. 116 (1) (2017) 295–318.
[25] A. Malvandi, D.D. Ganji, Effects of nanoparticle migration and asymmetric heating on magnetohydrodynamic forced convection of alumina/water nanofluid in microchannels, Eur. J. Mech. B-Fluid 52 (2015) 169–184.

[26] A. Malvandi, M.H. Kaffash, D.D. Ganji, Nanoparticles migration effects on magneto-hydrodynamic (MHD) laminar mixed convection of alumina/water nanofluid inside microchannels, J. Taiwan Inst. Chem. E 52 (2015) 40–56.
[27] H.R. Ashorynejad, A. Zarghami, K. Sadeghi, Analyzing thermo-hydrodynamics of nanofluid flowing through a wavy U-turn channel, Int. J. Mech. Sci. 144 (2018) 628–638.
[28] M. Sheikholeslami, D.D. Ganji, R. Moradi, Forced convection in existence of Lorentz forces in a porous cavity with hot circular obstacle using nanofluid via Lattice Boltzmann method, J. Mol. Liq. 246 (2017) 103–111.
[29] S. Succi, The Lattice Boltzmann Equation for Fluid Dynamics and beyond, Oxford University Press, UK, 2001.
[30] M. Bouzidi, M. Firdaouss, P. Lallemand, Momentum transfer of a Boltzmann lattice fluid with boundaries, Phys. Fluids 13 (11) (2001) 3452–3459.
[31] R. Mei, D. Yu, W. Shyy, L-S Luo, Force evaluation in the lattice Boltzmann method involving curved geometry, Physical Rev. E 65 (4) (2002) 041203.
[32] X. He, et al., Analytic solutions of simple flows and analysis of nonslip boundary conditions for the lattice Boltzmann BGK model, J. Stat. Phys. 87 (1997) 115–136.
[33] I. Orlanski, A simple boundary condition for unbounded hyperbolic flows, J. Comput. Phys. 21 (3) (1976) 251–269.
[34] H.R. Ashorynejad, A. Zarghami, Magnetohydrodynamics flow and heat transfer of Cu-water nanofluid through a partially porous wavy channel, Int. J. Heat Mass Transf. 119 (2018) 247–258.
[35] S.K.P. Sanjeevi, A. Zarghami, J.T. Padding, Choice of no-slip curved boundary condition for lattice Boltzmann simulations of high-Reynolds-number flows, Phys. Rev. E 97 (2018), 043305.
[36] J. Buckles, T.J. Hanratty, R.J. Adrian, Turbulent flow over large-amplitude wavy surfaces, J. Fluid Mech. 140 (1984) 27–44.
[37] A.J. Goldman, R.G. Cox, H. Brenner, Slow viscous motion of a sphere parallel to a plane wall – I Motion through a quiescent fluid, Chem. Eng. Sci. 22 (1967) 637–651.